Control of myosin-I force sensing by alternative splicing

Joseph M. Laakso, John H. Lewis, Henry Shuman, and E. Michael Ostap[1]

Pennsylvania Muscle Institute and Department of Physiology, University of Pennsylvania School of Medicine, Philadelphia, PA 19104

Edited by Thomas D. Pollard, Yale University, New Haven, CT, and approved November 25, 2009 (received for review October 2, 2009)

Myosin-Is are molecular motors that link cellular membranes to the actin cytoskeleton, where they play roles in mechano-signal transduction and membrane trafficking. Some myosin-Is are proposed to act as force sensors, dynamically modulating their motile properties in response to changes in tension. In this study, we examined force sensing by the widely expressed myosin-I isoform, myo1b, which is alternatively spliced in its light chain binding domain (LCBD), yielding proteins with lever arms of different lengths. We found the actin-detachment kinetics of the splice isoforms to be extraordinarily tension-sensitive, with the magnitude of tension sensitivity to be related to LCBD splicing. Thus, in addition to regulating step-size, motility rates, and myosin activation, the LCBD is a key regulator of force sensing. We also found that myo1b is substantially more tension-sensitive than other myosins with similar length lever arms, indicating that different myosins have different tension-sensitive transitions.

ATPase | kinetics | optical tweezers | single molecule | molecular motor

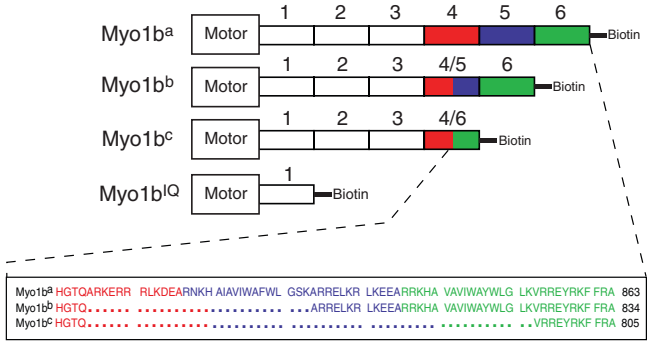

Fig. 1. Expressed myo1b protein constructs. Diagrams show the relationship of the myo1b motor domain (large rectangles) to the IQ motifs (smaller numbered rectangles). The IQ motifs that are alternatively spliced are colored, and the inset shows the amino acid sequences of the splice locations within IQ motifs 4–6. The small black rectangle corresponds to the 15 amino acid sequence that is biotinylated via biotin ligase.

Tension sensing by myosin motors is important for numerous cellular processes, including control of force and energy utilization in contracting muscles (1), transport of cellular cargos (2, 3), detection of auditory stimuli (4), and control of cell shape (5). Myosins have evolved different tension sensitivities tuned for these diverse cellular tasks (6), thus it is important to determine the mechanisms and regulation of force sensing within the myosin superfamily.

We recently demonstrated that the widely expressed myosin-I isoform, myo1b, is exquisitely sensitive to tension (7). Myo1b transitions from a low duty-ratio to a high duty-ratio motor at very low opposing forces (<1 pN). Evidence suggests that tension sensing occurs as stress on actomyo1b prevents the rotation of the myo1b lever arm, which inhibits ADP release and subsequent ATP binding and actin detachment (2, 7, 8).

Myo1b is alternatively spliced during development and in various tissues within its LCBD, which is the region of the motor that acts as the lever-arm (9). Splicing yields proteins with six (myo1b^a), five (myo1b^b), or four (myo1b^c) nonidentical calmodulin-binding IQ motifs that are spliced such that the fourth IQ motif exists as a hybrid with IQ-5 or IQ-6 in the two shorter isoforms (Fig. 1). The LCBD is a key mechanical component in the force production pathway (10, 11), so alternative splicing may be a mechanism to tune the mechanical properties of myo1b to varied physiological needs without changing basal ATPase kinetic or cargo-binding properties of the motor. Indeed, myosins II and V have different sized LCBDs and display different force sensitivities (2, 8). Therefore, we tested the possibility that alternative splicing regulates the tension sensitivities of recombinant myo1b splice isoforms. Because characterization of myosins with different length LCBDs provides an opportunity to better define the molecular basis of force sensing in all myosins, we also investigated the mechanical properties of a construct that contains a single IQ motif (myo1b^{IQ}) (Fig. 1).

Results

Step and Substep Sizes of Myo1b Splice Isoforms. Single actomyosin interactions were acquired using the three-bead configuration (12, 13), in which a single actin filament, suspended between two beads held by separate optical traps, is brought close to the surface of a pedestal bead that is sparsely coated with myo1b. Myo1b proteins were site-specifically attached to the streptavidin-coated pedestal beads via a biotinylation tag positioned directly C-terminal to the LCBD (14). Step sizes of the myo1b proteins were determined at low trap stiffnesses (~0.022 pN/nm) to minimize stress on the actomyo1b during the working stroke. A low ATP concentration (1 μM) was used in the step-size measurements to prolong actin attachments, allowing for clear identification of unitary interactions and precise determination of step sizes (7). A stage-position feedback system was also used to decrease low-frequency vibrations that were previously apparent in long actin attachments (7) (Fig. S1).

The myo1b working-stoke occurs in two substeps, with the first and second substeps most likely accompanying phosphate and ADP release, respectively (7, 15). Thus, we recorded working stroke displacements 50 ms after attachment and 50 ms before detachment and plotted distributions of total and substep sizes (Fig. 2*A*). We also determined average step sizes by ensemble averaging the time courses of unitary interactions (Fig. 2*B*) (8). Ensemble averages created by synchronizing interactions at their start times report the displacement of the first substep,

Author contributions: J.M.L., H.S., and E.M.O. designed research; J.M.L. and E.M.O. performed research; J.M.L., J.H.L., H.S., and E.M.O. contributed new reagents/analytic tools; J.M.L., J.H.L., H.S., and E.M.O. analyzed data; and J.M.L., J.H.L., H.S., and E.M.O. wrote the paper.

The authors declare no conflict of interest.

This article is a PNAS Direct Submission.

[1]To whom correspondence should be addressed. E-mail: ostap@mail.med.upenn.edu.

This article contains supporting information online at www.pnas.org/cgi/content/full/0911426107/DCSupplemental.

www.pnas.org/cgi/doi/10.1073/pnas.0911426107

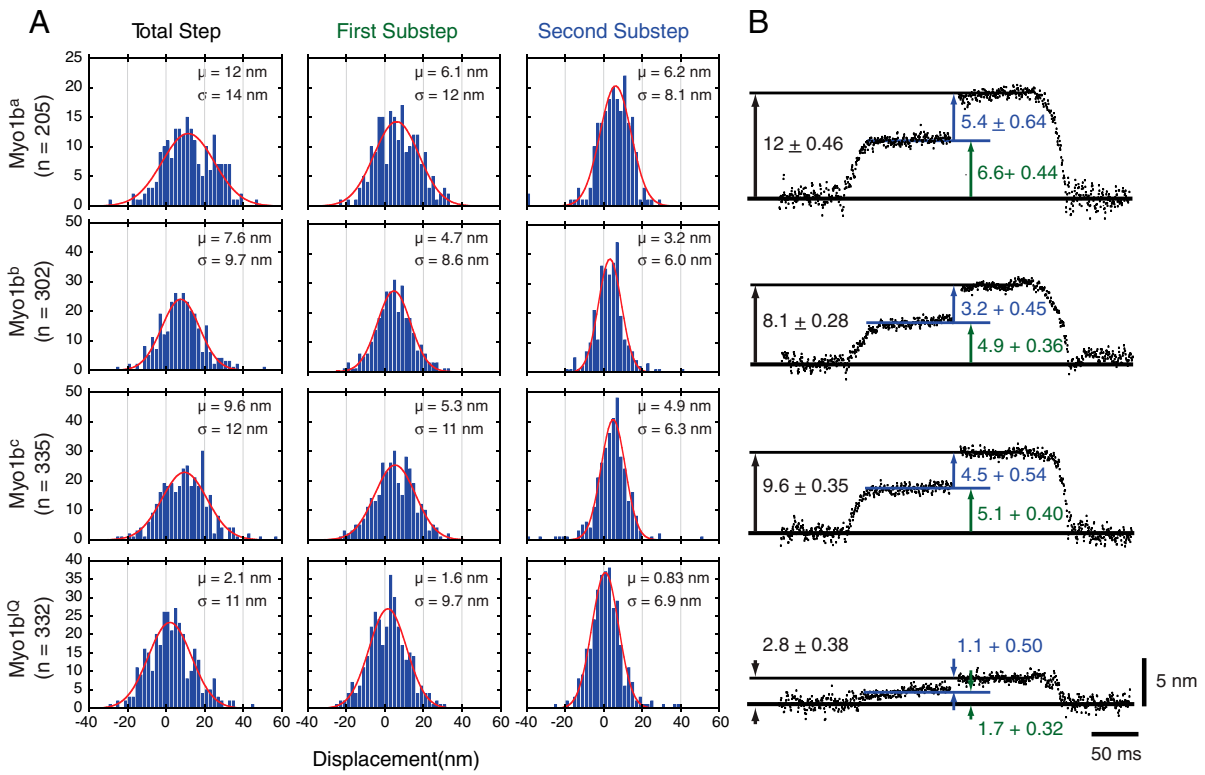

Fig. 2. Step and substep averages and distributions of myo1b splice isoforms. (*A*) Histograms of step and substep sizes of unitary interactions acquired in the presence of 1.0 μM ATP. The size of the first substeps of the individual interactions were calculated by averaging 100 points (50 ms of data), 50 ms after attachment. Total step sizes from each interaction were determined by averaging 100 points, 50 ms before detachment. The difference between the two measurements is reported as the second substep. Distributions were fit to a Gaussian function where μ and σ report the means and standard deviations of the Gaussian distributions, respectively. Standard errors of the Gaussian fits are reported in Table S1. Interactions were acquired from multiple coverslips as follows: myo1b^a (4), myo1b^b (6), myo1b^c (6), myo1b^{IQ} (5). (*B*) Ensemble averages showing the average step and substep sizes. Total step (black arrows), first substep (green arrows), and second substep (blue arrows) sizes obtained from the ensemble averages are reported. The uncertainty is the standard deviation of the 100 averaged data points (50 ms) from the ensemble trace.

and those synchronized at their end times report the overall step size (Fig. 2*B*).

The distributions of steps and substeps of individual interactions are well described by broad Gaussian distributions that center on values that are similar to the average displacements obtained by ensemble averaging (Fig. 2). Subpopulations are not apparent in the distributions, so the ensemble averaged traces are likely reporting the mean behavior of the unitary events. The standard deviations of the distributions of the first substeps are broader than the second substeps (Fig. 2*A*, Table S1). This broadening is likely due to variability in the positions on the actin filaments to which myosins bind prior to the first substep.

Total step and substep sizes are not linearly related to the number of IQ motifs in the constructs (Fig. 3), as found for other myosins (16). Total step size of myo1b^c is significantly larger than myo1b^{IQ} ($p < 0.0001$, unpaired two-tailed t-test), but total myo1b^b displacements are smaller than myo1b^c ($p = 0.090$), even though myo1b^b binds an additional calmodulin (14). If we assume that the LCBDs of myo1b^{IQ} and myo1b^c act as rigid lever arms, the slope of a line drawn between their total steps would predict a step size of ~15 nm for myo1b^b, which is 1.7-fold larger than experimentally determined. A projection of the actual myo1b^b step-size to this line results in the prediction that myo1b^b has an LCBD with an effective length of ~3 IQ motifs (Fig. 3, dashed line). Projection of the myo1b^a step size to the same line predicts an LCBD length of ~5 IQ motifs. Thus, as measured under the low-load conditions of the experiment, it appears that the IQ-5 and the first half of IQ-6 introduce a structural feature into the LCBD that decreases the effective lever arm size. We demon-

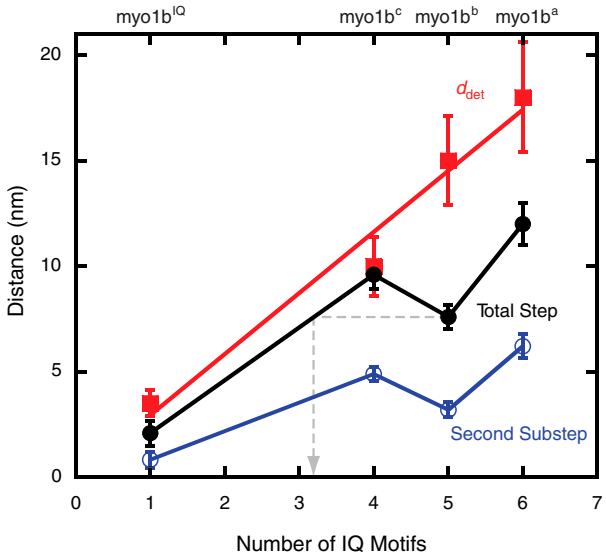

Fig. 3. Summary of step sizes and distance parameters of myo1b splice isoforms. Step sizes (circles) and distance parameters (squares) plotted as a function of the number of IQ motifs in the LCBD. Total (closed symbols) and second substep (open symbols) sizes are obtained from the fits to the Gaussian distributions as described in Fig. 2. The same protein preparations were used to acquire step sizes and distance parameters. The red line is a linear fit to the d_{det} points, giving a slope of 2.9 nm/IQ and a *y*-intercept of 0.054 nm ($r = 0.985$). Step and substep sizes are reported as the mean and standard errors of the mean, and d_{det} values are best fits showing 90% confidence limits.

BIOCHEMISTRY

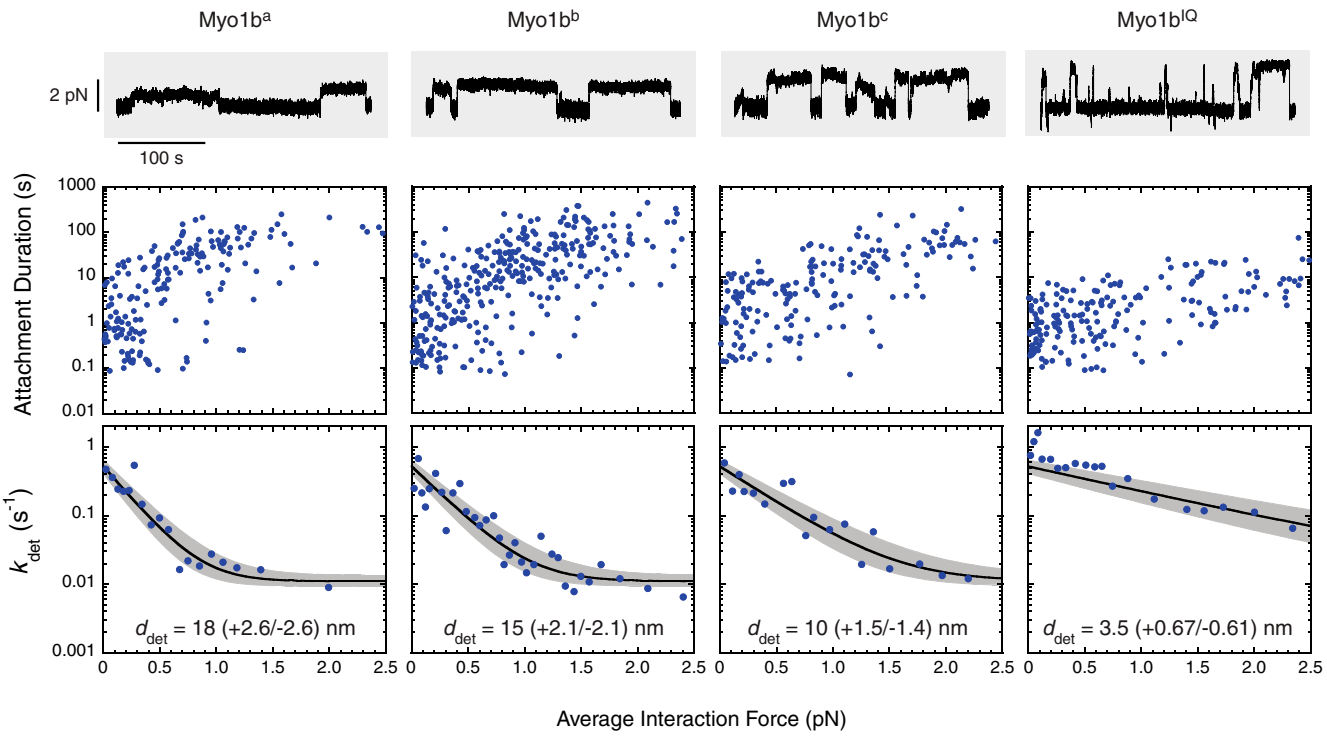

Fig. 4. Force dependence of myo1b splice isoform kinetics. (*Top Row*) Representative time traces showing force during unitary actomyo1b attachments acquired with the isometric clamp in the presence of 50 μM ATP. (*Center Row*) Attachment durations as a function of the average force during the attachment. Interactions were acquired from multiple coverslips as follows: myo1b^a (5), myo1b^b (6), myo1b^c (6), myo1b^{IQ} (4). (*Bottom Row*) Force dependence of the actin-detachment rates (k_{det}) as calculated using the parameters obtained by fitting the attachment durations by maximum likelihood estimation. The best fit values are $k_{g0} = 0.51(\pm 0.11)\ s^{-1}$, $k_i = 0.011(+0.0025/-0.0017)\ s^{-1}$, and d_{det} values are given in the figure. Points are the inverse averages of 10 consecutive attachment durations. The shaded areas show the 90% confidence limit based on the uncertainties.

strated previously that these IQ motifs have a weaker affinity for calmodulin (14).

Force-Dependent Actin-Detachment Kinetics. We measured the force-dependence of actomyo1b attachment durations using a feedback system that applies a dynamic load to the actomyo1b to keep the actin near its isometric position (Fig. 4) (7, 13). Experiments were performed in the presence of 50 μM ATP to ensure that the rate of ATP binding did not limit the rate of detachment (7, 17). Long attachment durations at higher forces are apparent in the time traces of all four myo1b proteins, but it is clear that the shorter isoforms have shorter attachment durations (Fig. 4).

Attachment durations of myo1b^a, myo1b^b, and myo1b^c increased until a plateau was reached, at which point the attachment durations appear to be force-independent (Fig. 4). The force at which this plateau is reached increases with decreasing number of IQ motifs. The attachment durations of myo1b^{IQ} are substantially less force-dependent, and a plateau is not as apparent over the range of forces probed in these experiments.

We modeled actomyo1b detachment with force-dependent (k_g) and force-independent rates (k_i):

$$\begin{array}{l}\text{Attached} \overset{k_g}{\rightarrow} \text{Detached} \\ k_i\downarrow \\ \text{Detached}\end{array}$$

and the force dependence of the detachment rate (k_{det}) was calculated as

$$k_{det}(F) = k_{g0}e^{-\frac{F \cdot d_{det}}{kT}} + k_i \qquad [1]$$

where k_{g0} is the rate of k_g in the absence of force, F is force, k is the Boltzmann constant, T is temperature, and d_{det} is the distance parameter, which reports the distance to the transition state of the force-sensitive step and is a measure of force sensitivity (7, 18).

Since the attachment durations are expected to be exponentially distributed at each force (Eq. **1**), we fit the data and determined the confidence limits using a maximum likelihood routine that uses a modified exponential probability distribution function (see *Methods*). We globally fit the four attachment-duration datasets to determine isoform-specific values for d_{det} with the assumption that k_{g0} and k_i are the same for the four proteins (Fig. 4).

The best fit d_{det} values for the four myo1b constructs are different and are linearly related to the number of IQ motifs (Fig. 3). The effect of these differences on the force dependencies is clearly illustrated via plots of k_{det} versus force (Fig. 4) and via plots of the dependence of attachment lifetime on splice isoform and force (Fig. 5). Myo1b^a, myo1b^b, and myo1b^c are extraordinarily force-sensitive, with k_{det} decreasing 10-fold within <0.25 pN of resisting force (Fig. 4). Myo1b^{IQ} is substantially less force-sensitive, requiring >2.5 pN resisting force to obtain a 10-fold decrease in k_{det}.

The best fit value of k_{g0} $(0.51(\pm 0.11)\ s^{-1})$ from the global fit is within ~2-fold of the rate of ADP release in the absence of load as measured by biochemical methods ($1.0\ s^{-1}$, 22 °C) (17), and the value obtained for k_i $(0.011(+0.0025/-0.0017)\ s^{-1})$ is within twofold of the value determined previously for myo1b^b ($k_i = 0.021\ s^{-1}$) (7).

Force-Independent Actin-Detachment Kinetics. We previously proposed that the force-independent detachment pathway (Scheme 1) is the result of accelerated actin detachment due

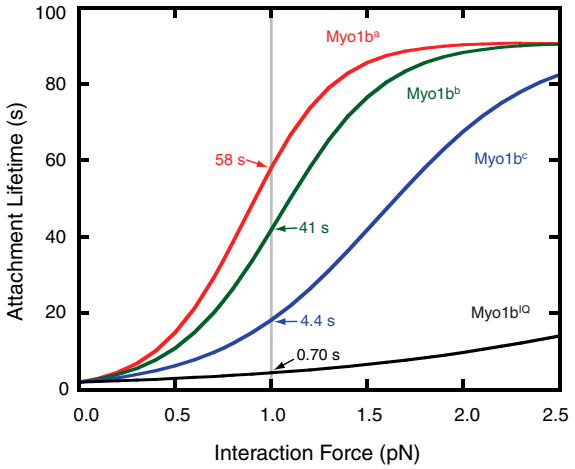

Fig. 5. Force dependence of attachment lifetimes of the myo1b splice isoforms. Attachment lifetimes ($1/k_{det}$) of the four myo1b protein constructs were calculated using the values obtained from the MLE fit of the data in Fig. 4 to Eq. 1. The inset numbers indicate explicit values of attachment lifetimes at 1 pN opposing force (gray line).

to low-frequency force fluctuations in the instrumentation (7). However, use of a stage feedback system that effectively removes this noise did not eliminate the force-independent pathway or dramatically affect the rate of k_i. Thus, we investigated whether this pathway is the result of the basal detachment of myo1b from actin.

The rate of detachment of myo1b^{IQ} from pyrene-labeled actin was measured in the absence of force by stopped-flow kinetics (Fig. S2). The detachment rate in the presence of ADP ($k_{off} = 0.015 \pm 0.00011$ s^{-1}) is remarkably similar to the best fit value obtained for $k_i(0.011(+0.0025/-0.0017)$ s^{-1}), and is fourfold faster than in the absence of nucleotide ($k_{off} = 0.0036 \pm 0.00036$ s^{-1}). Therefore, we identify the force-independent detachment pathway (Scheme 1) as the dissociation of myo1b in an ADP-like state from actin.

Discussion

The key finding of these studies is that myo1b splice isoforms have significantly different force-dependent kinetics of actin detachment, and the d_{det} values are linearly related to the number of IQ motifs (Fig. 3). The d_{det} values are larger than the average displacements of the second substep (Fig. 3), indicating that the force-sensitive transition is not on a coordinate that is in line with this substep displacement. Interestingly, the d_{det} values for myo1b^{IQ} and myo1b^c are comparable in size to their overall step sizes (Fig. 3), suggesting that for these constructs, the force-sensitive transition has a trajectory similar to the overall power-stroke. The overall step sizes of myo1b^a and myo1b^b are smaller than the d_{det} values (Fig. 3), yet if the step sizes of myo1b^a and myo1b^b followed the same step-size trend as myo1b^{IQ} and myo1b^c, the values of the overall step sizes and distance parameters would be similar.

We propose that in the presence of load, myo1b^{IQ} and myo1b^c dwell in a strong-binding state with an ADP-like affinity in which the lever arm has not rotated, and the force-sensitive transition requires the rotation of the lever arm with a magnitude that is similar to the overall step size. This mechanism is different from what has been found for myosin II (8) and myosin V (2), which have d_{det} values that correlate well with the size of their ADP-release-coupled substeps. Thus, despite the similarity of myo1b's two-step working stroke to myosins II and V, myo1b likely dwells in a different conformational state under load which results in increased force sensitivity.

We do not know why d_{det} values for myo1b^a and myo1b^b are larger than their overall step sizes (Fig. 3). The IQ motifs spliced into myo1b^a and myo1b^b do not contain the isoleucine-glutamine or arginine-glycine pairs of residues that have been shown to contribute to the binding of the C- and N-terminal lobes of calmodulin, and binding measurements show that calmodulin affinities for these motifs are weaker than for the canonical motifs (14). However, stoichiometry measurements show that myo1b^b binds five calmodulins and myo1b^a binds 5–6 calmodulins at the calmodulin concentrations used in our experiments (20 μM) (14). Nevertheless, weak calmodulin binding to the spliced IQ motifs may indicate an unusual LCBD structure, which may result in the shorter than expected step sizes at low loads. It is unlikely that the structural features introduced via splicing result in increased step sizes with load (which might lead to larger d_{det} values), as plots of the second substep size as a function of force do not show load-dependent step-size increases for any of the constructs (Fig. S3). Rather, splicing may introduce a "hook" or a "bend" in the LCBDs of myo1b^a and myo1b^b that may amplify torsional motions of the LCBD that are on the path to the transition state but are not apparent in the displacement measurements (19–21). Further structural and mechanical characterizations of the LCBD are required to resolve this issue.

Our results indicate that alternative splicing increases the range of force sensitivities of the proteins translated from the myo1b gene. Given the very long actin-attachment lifetimes of myo1b under low loads (<1 pN, Fig. 4), we propose that myo1b's function is to generate and sustain tension for extended periods of time, rather than to rapidly transport cellular cargos. Alternative splicing tunes the mechanical properties of myo1b for diverse mechanical challenges, while maintaining the protein's basal kinetic and cargo-binding properties. These results highlight the crucial role of the LCBD in defining the force sensitivity of myosins. These results also reinforce the finding that there is diversity in the mechanisms of force sensing within the myosin superfamily (2, 8, 13).

Materials and Methods

Proteins and Reagents. Myo1b expression constructs were prepared as described (14). All myo1b splice isoform constructs were truncated after the final IQ motif in the light chain binding domain (Fig. 1). An additional nonnative construct (myo1b^{IQ}) consisting of the motor and first IQ motif was also prepared. A 15-amino acid AviTag sequence for site-specific biotinylation and a FLAG sequence for purification were inserted at the C termini of the four constructs (14, 22).

Myo1b constructs were expressed and purified from Sf9 cells that were coinfected with virus containing recombinant myo1b and calmodulin as described (23). Concentrated protein was site-specifically biotinylated with 20 μg/ml biotin ligase in the presence of 10 mM MgATP and 50 μM biotin at 30 °C for 1 h. Free biotin and ATP were removed by MonoQ column chromatography and dialysis. Protein integrity was assessed by a standard motility assay (14, 24). The same protein preparations were used to acquire step sizes and distance parameters, thus the lower myo1b^b step size is not the results of inadvertent switching of isoforms.

Rabbit skeletal muscle actin was prepared as described (25). Actin concentrations were determined by absorbance at 290 nm, $\varepsilon_{259} = 26,600$ M^{-1} cm^{-1}. Actin for transient kinetics experiments was labeled with pyrenyl iodoacetamide (pyrene-actin) and gel filtered (26). All actin was stabilized with a molar equivalent of phalloidin (Sigma). Calmodulin was expressed in bacteria and purified as described (27).

Single-Molecule Measurements. Single-molecule interactions were recorded using the three-bead assay geometry in a dual-beam optical trap system as described (7, 13). Beads and motility chambers were prepared as described in *SI Text*. Trap stiffnesses were ~0.022 pN/nm. *N*-ethylmaleimide (NEM) myosin-II beads were captured in separate optical traps, and bead-actin-bead dumbbells were assembled by contacting the trapped beads with single actin filaments. Bead-actin-bead assemblies were pretensioned to ~2.5 pN and lowered onto the surface of a pedestal using a piezoelectric stage controller to scan for actomyo1b interactions. Upon observation of interactions, data were digitized with a 2 kHz sampling rate for 6–10 min intervals. All

experiments were performed in KMg 25 (10 mM Mops, 25 mM KCl, 1 mM $MgCl_2$, 1 mM EGTA, 1 mM DTT).

The force dependence of actomyo1b attachment lifetimes was measured using a feedback system that applies a dynamic load to the actomyo1b to keep the actin filament near its isometric position during the myosin working stroke as described (7, 13). Briefly, changes in the force on the bead attached to the pointed end of the actin filament (transducer bead) were fed through an analog integrating feedback amplifier to an acousto-optic deflector, which changed the position of the laser trap on the bead bound to the barbed end of the actin filament (motor trap) until the position of the transducer bead was restored to its original position. The response time of the feedback loop in the absence of interactions was adjusted to 50 ms for each bead-actin-bead assembly.

To control low-frequency stage-position fluctuations, an additional infrared laser beam ($\lambda = 830$ nm, Point-Source) was installed on the same beam path as the trapping laser, with the exception that after being collected and collimated by the condenser objective, the laser light was directed to a separate 4-quadrant photodiode. We monitored the position of the pedestal on which the myo1b is attached, and controlled the *x*-axis (i.e., the long axis of the actin filament) of the stage position using an analog integrating feedback amplifier. By incorporating this stage feedback system into our experiments, we can reduce fluctuations of the stage due to drift or mechanical vibration, thus reducing the noise in our force traces (Fig. S1).

The start and endpoints of actomyo1b attachments were determined as described in *SI Text*. The best values for the parameters described in Eq. **1** were found using a maximum likelihood routine utilizing a modified exponential decay probability distribution function (28). The log likelihood was minimized with a Nelson-Mead downhill simplex routine (28). The function was sufficiently complex that the minimization had to be frequently restarted in order to find the true global minimum. The restart algorithm was modified from an annealing routine sometimes used for multiple parameter fits (28). The combination of these two algorithms allowed for a rapid convergence to the global minimum of the log likelihood function. Confidence intervals for each uniquely determined parameter were found by simulating the data with a bootstrap routine (28). We generated 1,000 such datasets and independently fit them for all of the relevant parameters. In order to calculate the confidence interval of 90% for a given parameter, the boundaries were determined in which 45% of the simulated data were contained on either side of the value of the parameter from the actual data. The maximum and minimum confidence interval were then calculated from the upper and lower boundaries, respectively.

Actomyo1b Dissociation Experiments. The detachment rates of myo1b^{IQ} from pyrene-actin were determined with an Applied Photophysics (Surrey, U.K.) SX.18MV stopped-flow fluorometer in the absence and presence of 25 μM ADP. A 400 nm long-pass filter (Oriel) was used to monitor pyrene ($\lambda_{ex} = 365$ nm) fluorescence. Dissociation experiments were performed by mixing 0.5 μM pyrene-actomyo1b^{IQ} with 50 μM unlabeled actin (final concentrations after mixing). Times courses of averaged experimental transients were fitted to a single exponential function using the software supplied with the stopped-flow. Reported errors are the standard error of the fit.

ACKNOWLEDGMENTS. We thank Tianming Lin for outstanding technical assistance, and Dr. Yale E. Goldman for helpful discussions. This work was support by grants from the National Institutes of Health (GM57247 and AR051174). J.H.L. was supported by a National Institute of Arthritis and Musculoskeletal and Skin Diseases training grant (AR053461).

1. Fenn WO (1923) A quantitative comparison between the energy liberated and the work performed by the isolated sartorius muscle of the frog. *J Physiol-London*, 58:175–203.
2. Veigel C, Schmitz S, Wang F, Sellers JR (2005) Load-dependent kinetics of myosin-V can explain its high processivity. *Nat Cell Biol*, 7(9):861–869.
3. Altman D, Sweeney HL, Spudich JA (2004) The mechanism of myosin VI translocation and its load-induced anchoring. *Cell*, 116(5):737–749.
4. Gillespie PG (2004) Myosin I and adaptation of mechanical transduction by the inner ear. *Philos TR Soc Lon B*, 359(1452):1945–1951.
5. Ren Y, et al. (2009) Mechanosensing through cooperative interactions between myosin II and the actin crosslinker cortexillin I. *Curr Biol*, 19(17):1421–1428.
6. Kee YS, Robinson DN (2008) Motor proteins: Myosin mechanosensors. *Curr Biol*, 18(18):R860–862.
7. Laakso JM, Lewis JH, Shuman H, Ostap EM (2008) Myosin I can act as a molecular force sensor. *Science*, 321(5885):133–136.
8. Veigel C, Molloy JE, Schmitz S, Kendrick-Jones J (2003) Load-dependent kinetics of force production by smooth muscle myosin measured with optical tweezers. *Nat Cell Biol*, 5(11):980–986.
9. Ruppert C, Kroschewski R, Bahler M (1993) Identification, characterization and cloning of myr 1, a mammalian myosin-I. *J Cell Biol*, 120(6):1393–1403.
10. Rayment I, et al. (1993) Three-dimensional structure of myosin subfragment-1: A molecular motor. *Science*, 261(5117):50–58.
11. Warshaw DM (2004) Lever arms and necks: A common mechanistic theme across the myosin superfamily. *J Muscle Res Cell Motil*, 25(6):467–474.
12. Finer JT, Simmons RM, Spudich JA (1994) Single myosin molecule mechanics: Piconewton forces and nanometre steps. *Nature*, 368(6467):113–119.
13. Takagi Y, Homsher EE, Goldman YE, Shuman H (2006) Force generation in single conventional actomyosin complexes under high dynamic load. *Biophys J*, 90(4):1295–1307.
14. Lin T, Tang N, Ostap EM (2005) Biochemical and motile properties of Myo1b splice isoforms. *J Biol Chem*, 280(50):41562–41567.
15. Veigel C, et al. (1999) The motor protein myosin-I produces its working stroke in two steps. *Nature*, 398(6727):530–533.
16. Warshaw DM, et al. (2000) The light chain binding domain of expressed smooth muscle heavy meromyosin acts as a mechanical lever. *J Biol Chem*, 275(47):37167–37172.
17. Lewis JH, Lin T, Hokanson DE, Ostap EM (2006) Temperature dependence of nucleotide association and kinetic characterization of myo1b. *Biochemistry*, 45(38):11589–11597.
18. Bell GI (1978) Models for the specific adhesion of cells to cells. *Science*, 200 (4342):618–627.
19. Jontes JD, Milligan RA (1997) Brush border myosin-I structure and ADP-dependent conformational changes revealed by cryoelectron microscopy and image analysis. *J Cell Biol*, 139(3):683–693.
20. Sabido-David C, et al. (1998) Orientation changes of fluorescent probes at five sites on the myosin regulatory light chain during contraction of single skeletal muscle fibres. *J Mol Biol*, 279(2):387–402.
21. Hopkins SC, Sabido-David C, Corrie JE, Irving M, Goldman YE (1998) Fluorescence polarization transients from rhodamine isomers on the myosin regulatory light chain in skeletal muscle fibers. *Biophys J*, 74(6):3093–3110.
22. Schatz PJ (1993) Use of peptide libraries to map the substrate specificity of a peptide-modifying enzyme: A 13 residue consensus peptide specifies biotinylation in Escherichia coli. *Biotechnology (N Y)*, 11(10):1138–1143.
23. El Mezgueldi M, Tang N, Rosenfeld SS, Ostap EM (2002) The kinetic mechanism of Myo1e (human myosin-IC). *J Biol Chem*, 277(24):21514–21521.
24. Kron SJ, Spudich JA (1986) Fluorescent actin filaments move on myosin fixed to a glass surface. *Proc Natl Acad Sci USA*, 83(17):6272–6276.
25. Spudich JA, Watt S (1971) The regulation of rabbit skeletal muscle contraction I. Biochemical studies of the interaction of the tropomyosin-troponin complex with actin and the proteolytic fragments of myosin. *J Biol Chem*, 246(15):4866–4871.
26. Pollard TD (1984) Polymerization of ADP-actin. *J Cell Biol*, 99(3):769–777.
27. Putkey JA, Slaughter GR, Means AR (1985) Bacterial expression and characterization of proteins derived from the chicken calmodulin cDNA and a calmodulin processed gene. *J Biol Chem*, 260(8):4704–4712.
28. Press WH, Teukolsky SA, Vetterling WT, Flannery BP (2002) *Numerical Recipes in C++* (Cambridge Univ Press, New York).